# Bolted and hybrid beam-column joints between I-shaped FRP profiles

J. Qureshi
*School of Architecture, Computing and Engineering, University of East London, London E16 2RD, UK*

Y. Nadir and S. K. John
*Department of Civil Engineering, College of Engineering Trivandrum, Thiruvananthapuram, Kerala, India*

ABSTRACT: Presented are test results from five full-scale pultruded FRP beam-to-column joints subjected to cyclic loading. The parameters include cleat position, connection method and cleat material. The joints' behaviour is assessed through hysteresis moment rotation loops, accumulated dissipated energy and failure patterns. The hybrid joints with steel cleats showed the best overall cyclic performance with accumulated dissipated energy 75% higher than the bolted joint. The bolted joint with FRP cleats exhibited the lowest dissipated energy, four times lower than the joint with steel cleats. The cyclic performance of web and flange cleated joint was same as flange cleated joint. Three failure patterns were noticed, namely shear-out failure of the beam's bolted region (bolted joint with steel cleats), adhesive debonding followed by shear-out failure (hybrid joint with steel cleats) and delamination cracking (bolted joint with FRP cleats).

## 1 INTRODUCTION

Buildings and construction produce a third of global carbon emissions. For lower ecological impact, there is a need to promote sustainable materials for dealing with climate emergency (Qureshi & Mottram 2014). Fibre reinforced polymer is such eco-friendly material. It has superior durability, corrosion resistance, lower ecological impact and whole life-cycle cost, lightweight, and aesthetic possibilities. Typical applications of FRP in Civil Engineering include cooling towers, chemical and food processing plants, railway platforms and footbridges.

FRP composites contain carbon or glass fibres embedded in a polyester or vinylester resin matrix. The material properties in the longitudinal direction are three times higher than transverse direction. Tensile strength in longitudinal direction is 200-300 MPa with elastic modulus of 20-30 GPa. Standard FRP profiles, I, H and L, are produced through pultrusion process (Bank 2006; Zafari et al. 2016; Qureshi et al. 2020).

Joints between FRP profiles can be bolted or adhesively bonded. Bolting leads to discontinuity of fibres and bonding is affected by environmental factors. Combining both bolting and bonding (hybrid) alleviates weaknesses of the joining methods. Hybrid joints are effective in resisting loads in different directions – adhesive in direct tension and bolting in transverse direction. They provide a fail-safe mechanism against fire, fatigue, and long-term loading (Anonymus 1999; Kelly 2006).

Previous research is mainly focused on FRP joints under monotonic loading only (Turvey & Cooper 1996; Mottram & Zheng 1999; Qureshi & Mottram 2013; Qureshi & Mottram 2015). Limited research exists on cyclic response of FRP beam-column joints (Zhang et al. 2018; Razaqpur et al. 2019; Martins, Figueiredo Sá, et al. 2019; Martins, Proença, et al. 2019; Qiu et al. 2020; Martins et al. 2021). And that too is related to FRP tubular joints. Only few publications (Bruneau & Walker 1994; Martins et al. 2021) on cyclic response of joints between FRP I-shaped profiles exist. Further research is required on cyclic behaviour of FRP joints to assess seismic performance of FRP structures better.

This paper aims to investigate cyclic response of FRP joints between I-shaped sections. Five full-scale physical tests are performed. The test parameters include cleat material (steel or FRP), position of cleats (Flange or web cleated) and joining method (bolted or hybrid).
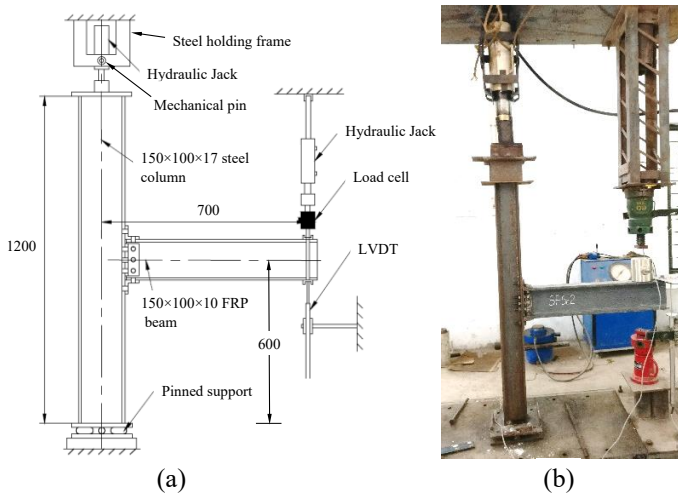
Figure 1. Test configuration: (a) Schematic diagram; (b) Photograph of beam-column sub-assembly

## 2  TEST CONFIGURATION

Figure 1 shows a single-sided beam-to-column joint sub-assembly test arrangement used in this study. The joint is between a beam profile of 150×100×10 mm pultruded FRP section and a steel column of ISWB 150×100×17 kg/m size. The cleat (steel or FRP) size is 50×50×6 mm leg-angles. A steel grade of Fe410 with a yield and ultimate strength of 250 MPa and 410 MPa is used for steel components. Grade 8.8 M12 threaded bolts are used.

Test labelling uses a four-letter format. First three letters show column, beam and cleat material ('S' for steel and 'F' for FRP). The fourth small letter indicates joint configuration, either 'c' for flange and web cleated or 'tc' for flange cleated only. The number can be '1' for monotonic loading and '2' for cyclic loading. The last letter, 'A', is for adhesive bonding in addition to bolting (hybrid joint). Five tests under cyclic loading are presented in this study; and companion monotonic tests are reported in (Qureshi et al. 2020).

There are five tests: SFSc2 – bolted joint with web and flange steel cleats; SFSc2A – companion hybrid joint; SFStc2 – bolted joint with steel flange cleats only; SFStc2A – companion hybrid joint and SFFc2 – bolted joint with web and flange FRP cleats. Figure 2 shows typical joint detailing for specimen SFSc2A.
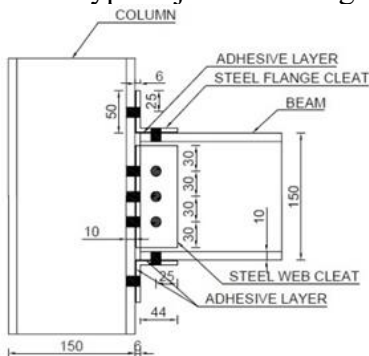


Figure 2. Typical joint detailing: Specimen SFSc2A

As there is no specific guide for joints under cyclic loading, the joint detailing is as per Eurocomp (Clarke 1996) and IS 800 (IS 800 2007). The joints are either bolted or 'hybrid' combining both bolting and bonding. Adhesive bonding uses multi-purpose epoxy resin AW 106 and hardener HV 953 U IN by Araldite®. The hydraulic jack that loaded the beam had a capacity of 500 kN with a stroke of ±150 mm with a load cell attached with a capacity of 50 kN and a resolution of ±0.02 kN. Two 100 mm LVDTs, with a resolution of ±0.01 mm, were used to measure displacements. Another hydraulic jack, with a capacity of 250 kN and a travel of 150 mm, was used to apply the compressive load to the column.

Before loading the beam, a constant compression load of 20% of the column's axial capacity was applied to the column to hold the column in position. This replicates the real-life situation, where columns support gravity loads. As the failure is likely to happen in either cleats or the beam's bolted zone, the compressive load on steel column will not affect the joint's response. The beam is loaded near free end via hanger assembly. Joint rotation was worked out from measured displacements.

The cyclic load was applied to the end of the cantilever beam by controlling displacement. Different cyclic loading protocols for testing steel structures (ATC-24 and SAC), wood structures (ISO and CUREE) and non-structural elements (FEMA-461 and FM-1950) have been used in the past (Filiatrault et al. 2018). But these protocols use yield load as the criterion for cyclic load application. As FRPs do not have any clear yield load, we used SAC protocol (SAC 1997), which is based on deformation rather than yield loading. In this paper, the inter-storey drift angle (total rotation), defined as displacement of loading point divided by distance between load point and centre of the column, is used to control the loading history. The cyclic loading history consists of stepwise symmetric displacement cycles as shown in Figure 3.
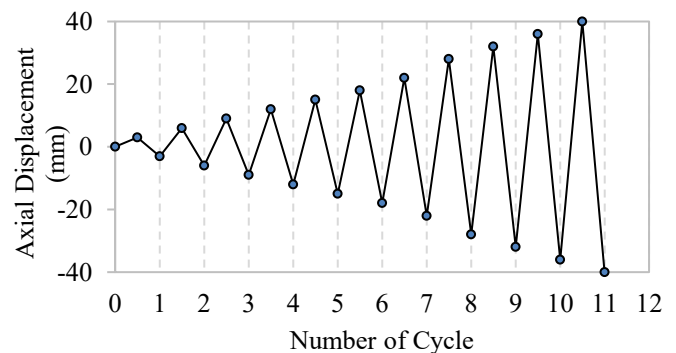


Figure 3. Cyclic loading history as SAC (SAC 1997) protocol

## 3 RESULTS AND DISCUSSION

This section presents moment-rotation hysteresis curves, accumulated dissipated energy for cyclic performance and failure modes.

### 3.1 *Moment-rotation hysteresis curves*

Moment-rotation hysteresis curves are produced from cyclic loading. For comparison, moment-rotation curves from companion monotonic tests in (Qureshi et al. 2020) are also given in Figure 4. Moment-rotation hysteresis curves for each specimen under cyclic loading are presented in Figures 5-9. These figures also show companion monotonic moment-rotation response and cyclic backbone or reference skeleton curves. Backbone curves are produced by linking together peaks of full cycles. A full cycle comprises compression and tension half cycles. In Figures 5-9, monotonic curves are shown by dashed lines, cyclic curves by dotted lines and backbone curves by solid lines with markers.

The moment-rotation properties can be categorised into initial, damage onset and maximum values. First failure or damage onset is the point on a moment-rotation curve, where either cracking causing fibre exposure happened or loud cracking noise was first heard. Apparently, it could be taken as synonymous to a yield point in steel structures.

Figure 4 presents the moment-rotation curves from companion monotonic tests conducted earlier by the authors (Qureshi et al. 2020). The results showed that hybrid joints (bonded and bolted) exhibited 60% higher moment and stiffness than bolted only joints. Addition of web cleat to the flange cleated joint only enhanced stiffness without corresponding increase in the moment capacity. Use of steel cleats instead of FRP led to 50% increase in the moment capacity. Generally, hybrid joints exhibited higher rotational stiffness in moment-rotation plots than their bolted counterparts.
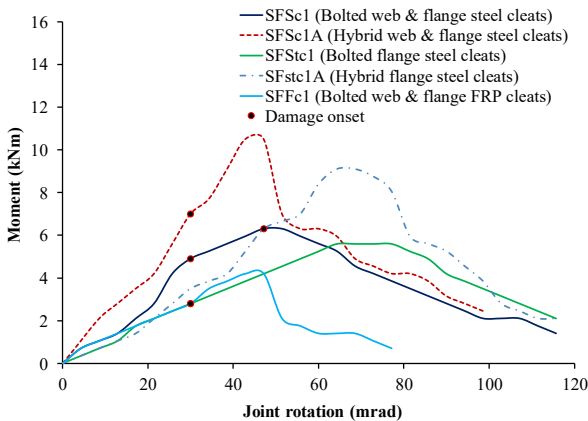


Figure 4. Moment-rotation curves for beam-column joints under monotonic loading, adapted from (Qureshi et al. 2020)

Figure 5 shows the moment-rotation response for the specimen SFSc2 (bolted joint with steel web and flange cleats). The backbone cyclic curve remained linear up to second loading cycle at $M_i$ of 1.4 kNm and $\phi_i$ of 8.6 mrad. Damage started during 5$^{th}$ compression half cycle after 4$^{th}$ increment (12 mm) with $M_j = 2.1$ kNm, $\phi_j = 17.1$ mrad. Maximum moment and rotation happened at the end of 8$^{th}$ cycle at 5.6 kNm and 37.1 mrad. First failure or damage onset occurred in monotonic tests at a moment 4.6 kNm and a rotation of 27.1 mrad. The damage in cyclic test happened much earlier than monotonic tests. The maximum properties in cyclic tests were also lower than monotonic tests.

Figure 6 presents the moment-rotation behaviour for the specimen SFSc2A (hybrid joint with steel web and flange cleats). The backbone moment-rotation curve remained linear until second loading cycle with moment of $M_i$ of 2.1 kNm and $\phi_i$ of 8.6 mrad. This time, first failure happened on the way to 5$^{th}$ tension half cycle at 4$^{th}$ displacement increment (12 mm) at a moment and rotation of -5.25 kNm and -17.1 mrad. In contrast, damage in monotonic tests happened much later at moment (7.0 kNm) and rotation (30.0 mrad). The specimen experienced the maximum moment (9.10 kNm) and rotation (37.1 mrad) at 8$^{th}$ cycle.
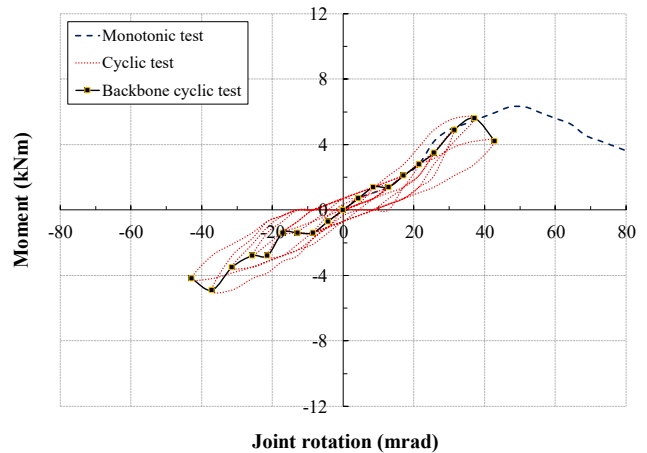


Figure 5. Cyclic moment-rotation hysteresis curves: SFSc2 – bolted joint with double web and flange steel cleats
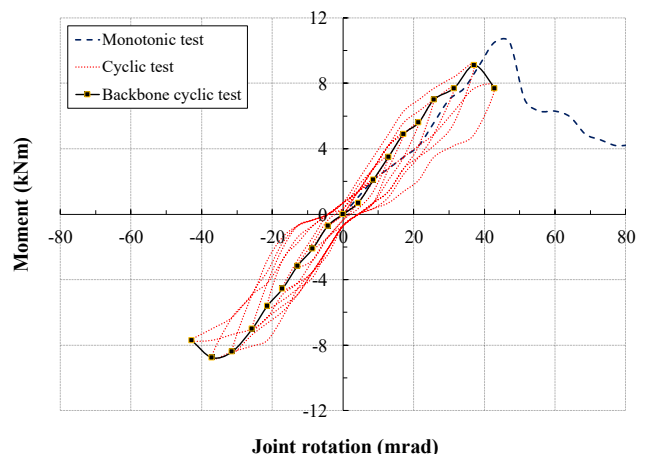


Figure 6. Cyclic moment-rotation hysteresis curves: SFSc2A – hybrid joint with double web and flange steel cleats
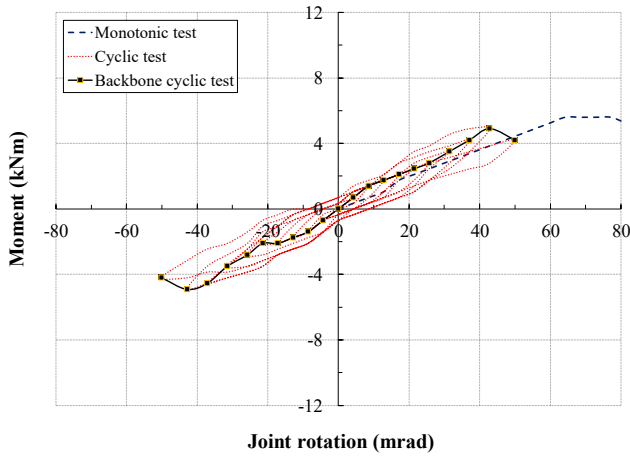
Figure 7. Cyclic moment-rotation hysteresis curves: SFStc2 – bolted joint with flange only steel cleats
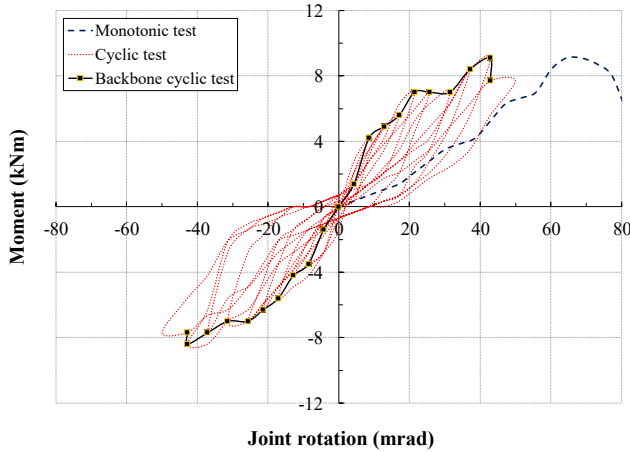


Figure 8. Cyclic moment-rotation hysteresis curves: SFStc2A – hybrid joint with flange only steel cleats



Figure 9. Cyclic moment-rotation hysteresis curves: SFFc2 – bolted joint with double web and flange FRP cleats
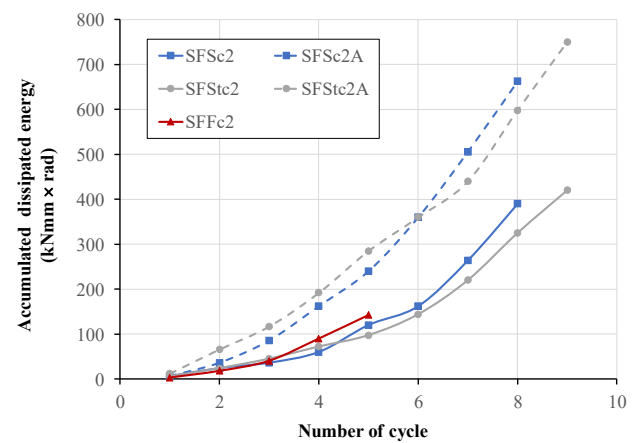


Figure 10. Accumulated dissipated energy of each joint against number of cycles

The specimen SFStc2 comprised the same joint as SFSc2, but without web cleats. It only had bolted flange cleats and moment-rotation hysteresis loops are given in Figure 7. The specimen had same linear joint properties as SFSc2. The damage started at the end of 4th compression half cycle at moment 2.1 kNm and rotation 17.1 mrad. The initial and damage joint properties were the same as in the specimen SFSc2 with web and flange cleats. Addition of double web cleats to a flange-only cleated bolted joint did not affect the moment-rotation response, at least at damage onset. It withstood a maximum moment of 4.9 kNm with rotation of 42.9 mrad at 9th loading cycle.

Figure 8 shows moment-rotation response of a companion test SFStc2A to SFStc2, with adhesive bonding in addition to bolting. The backbone moment-rotation curve remained linear up to second cycle with initial moment (4.2 kNm) and rotation (8.6 mrad). First failure started during 5th compression half cycle after 4th increment (12 mm) with $M_j = 6.3$ kNm and $\phi_j = 17.1$ mrad. The initial and damage stiffness were far higher than corresponding monotonic stiffnesses. The specimen had a maximum moment of 9.1 kNm with 42.9 mrad rotation at the end of 9th loading cycle.

Figure 9 presents moment-rotation response for SFFc2, the only specimen with FRP web and flange cleats. The backbone curve showed linear moment-rotation response until initial moment of 1.05 kNm and rotation of 8.6 mard. Damage started at the end of third compression half cycle, with moment reaching 1.75 kNm at a rotation of 12.86 mrad. Damage in monotonic test started far later than cyclic test at moment level of 2.8 kNm with 30 mrad rotation. The maximum moment attained was 3.5 kNm with rotation capacity of 21.43 mrad at 5th loading cycle. This is clearly less than 4.2 kNm moment achieved in the monotonic test at a rotation of 42.9 mrad.

## 3.2 Cyclic response

The cyclic performance of each specimen is evaluated by plotting the accumulated dissipated energy against number of cycles in Figure 10. The dissipated energy at each cycle is calculated as area enclosed by the moment-rotation hysteretic loop for each test. The accumulated dissipated energy is cumulative sum of each cycle. For example, 4th cycle is addition of dissipated energy from 1st to 4th cycles' moment-rotation hysteresis curve. The hybrid joints (SFSc2A and SFStc2A)

presented the best overall performance in terms of dissipated energy.

The final accumulated dissipated energy for specimen with hybrid joints, SFSc2A and SFStc2A, was about 70% and 78% higher than bolted only specimens SFSc2 and SFStc2. The energy performance of web and flange cleated, and flange cleated joints was almost similar. This reinforces our conclusion earlier that use of web cleats is redundant; flange only cleated joint will perform equally well. FRP cleated joint performed poorly with final accumulated dissipated energy about half of the corresponding joint with steel cleats.

## 3.3 Failure patterns

Depending on joint detailing and material strength, three failure modes were observed: shear-out failure of the beam's bolted region, adhesive debonding with shear-out failure in beam and delamination cracking of cleat. These are explained in following sections.

### 3.3.1 Shear-out failure at beam bolted zone

The shear-out failure happens when fibres are oriented mainly in the tension direction of the force or when the distance from bolt centreline to the free end of the beam is short. This failure mode happened in steel cleated bolted joints, SFSc2 and SFStc2, as shown in Figure 11. The shear-out was observed in the beam's flange and web regions below the neutral axis after dismantling the joint. The applied moment at the joint creates out-of-plane forces in the connected members. Due to cyclic loading, alternate prying and compressive forces cause shear-out failure in the beam flanges and web below neutral axis. The companion monotonic test also exhibited the same failure pattern.

### 3.3.2 Adhesive debonding with shear-out failure

For hybrid – adhesively bonded and bolted joints SFSc2A and SFStc2A, the failure was due to adhesive debonding in the cleated region of the beam followed by shear-out failure in the bolted region of the FRP beam. Figure 12 shows SFSc2A and SFStc2A joints at failure. The damage onset was identified by the visible cracking in the web-flange interface of the beam. The cracks progressed in the beam along with acoustic emissions in succeeding loading cycles.

After reaching the ultimate moment capacity, the adhesive layer failed suddenly with visible separation of the steel cleat from the FRP beam. The final failure was due to shear-out failure in bolted region of both flange and web of the beam. The adhesive bonding failed due to shear near the steel flange cleats by prying action. The shear-out failure in the beam was delayed by adhesive bonding. For monotonic loading, the cracking in the web-flange interface was comparatively less, but the ultimate failure remained same.

### 3.3.3 Delamination cracking

For the FRP cleated joint SFFc2, the failure was due to delamination cracks at the root radius of FRP cleats, as shown in Figure 13. Damage onset was observed by hairline cracks at the root radius of FRP flange cleats. The cracks propagated from the root radius leading to delamination of the cleats. The prying action led to the cracks at the top and bottom flange cleats due to out-of-plane bending caused by the applied moment. No cracks were observed in the members. The delamination failure was also observed in the web cleats, after dismantling the joint.



(a)　　　　　　　　　　　(b)
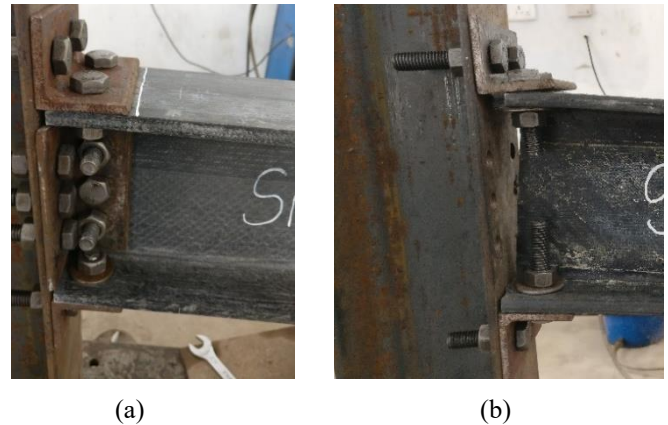
Figure 11. Shear-out failure at beam's bolted region: (a) Specimen SFSc2; (b) Specimen SFStc2



(a)　　　　　　　　　　　(b)
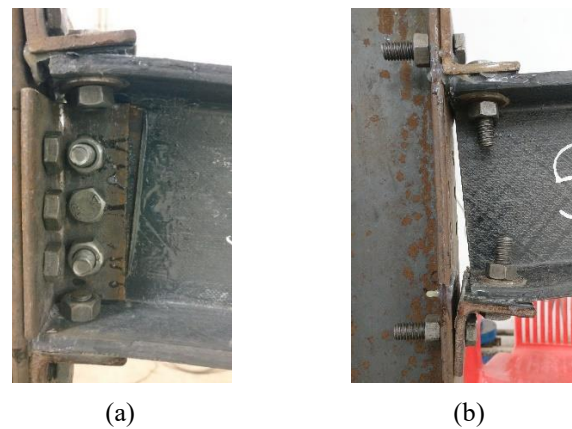
Figure 12. Adhesive debonding with shear-out failure: (a) Specimen SFSc2A; (b) Specimen SFStc2A



Figure 13. Delamination cracking in specimen SFFc2

# 4 CONCLUSIONS

Five full-scale joints are tested to study the cyclic behaviour of pultruded FRP beam-to-column joints between I-shaped profiles. The test parameters include cleat position, joining method and cleat material. Following conclusions can be drawn from this study:

- Three failure modes were observed: shear-out failure of the beam's bolted zone (bolted joints with steel cleats), adhesive debonding followed by shear-out failure of the beam (hybrid joint – bolting and bonding combined with steel cleats) and delamination cracking at the root radius of cleats (bolted joints with FRP cleats).
- The ratio of maximum over damage onset cyclic moment was about 2.5 for bolted joints and 1.5 for hybrid bonded and bolted joints. This indicates that adhesive bonding delays initiation of damage within FRP cleats and members.
- Hybrid joints showed twice as much stiffness as bolted joints, regardless of joint detailing. Bonding improved the connection stiffness, but without corresponding increase in the ultimate joint capacity.
- Adding web cleat to a flange cleated joint is redundant, as no increase in strength, stiffness, or accumulated energy was noticed.
- The hybrid joints with steel cleats gave excellent performance in terms of dissipated energy. The accumulated dissipated energy of hybrid joints was about 75% higher than bolted joints. The worst cyclic performance was shown by FRP cleated joint with accumulated dissipated energy only half of the steel cleated FRP joint.

REFERENCES

Anonymus. 1999. Guide to the structural use of adhesives. London, UK: Institution of Structural Engineers.

Bank LC. 2006. Composites for construction - Structural design with FRP materials. New Jersey, USA: John Wiley & Sons.

Bruneau M, Walker D. 1994. Cyclic testing of pultruded fiber-reinforced plastic beam-column rigid connection. J Struct Eng. 120(9):2637–2652.

Clarke JL. 1996. Structural Design of Polymer Composites-EUROCOMP Design Code and Handbook. [place unknown].

Filiatrault A, Perrone D, Brunesi E, Beiter C, Piccinin R. 2018. Effect of cyclic loading protocols on the experimental seismic performance evaluation of suspended piping restraint installations. Int J Press Vessel Pip. 166:61–71.

IS 800. 2007. General Construction in Steel - Code of Practice. [place unknown]: Bureau of Indian Standards.

Kelly G. 2006. Quasi-static strength and fatigue life of hybrid (bonded/bolted) composite single-lap joints. Compos Struct. 72(1):119–129.

Martins D, Figueiredo Sá M, Almeida Gonilha J, Ramôa Correia J, Silvestre N, Gomes Ferreira J. 2019. Experimental and numerical analysis of GFRP frame structures. Part 2: Monotonic and cyclic sway behaviour of plane frames. Compos Struct. 220:194–208.

Martins D, Gonilha J, Correia JR, Silvestre N. 2021. Exterior beam-to-column bolted connections between GFRP I-shaped pultruded profiles using stainless steel cleats. Part 1: Experimental study. Thin-Walled Struct. 163.

Martins D, Proença M, Almeida Gonilha J, Figueiredo Sá M, Ramôa Correia J, Silvestre N. 2019. Experimental and numerical analysis of GFRP frame structures. Part 1: Cyclic behaviour at the connection level. Compos Struct. 220:304–317.

Mottram JT, Zheng Y. 1999. Further tests on beam-to-column connections for pultruded frames: Flange-cleated. J Compos Constr. 3(1):3–11.

Qiu C, Bai Y, Cai Z, Zhang Z. 2020. Cyclic performance of splice connections for hollow section fibre reinforced polymer members. Compos Struct. 243:112222.

Qureshi J, Mottram JT. 2013. Behaviour of pultruded beam-to-column joints using steel web cleats. Thin-Walled Struct. 73:48–56.

Qureshi J, Mottram JT. 2014. Response of beam-to-column web cleated joints for FRP pultruded members. J Compos Constr. 18(2):04013039.

Qureshi J, Mottram JT. 2015. Moment-rotation response of nominally pinned beam-to-column joints for frames of pultruded fibre reinforced polymer. Constr Build Mater. 77:396–403.

Qureshi J, Nadir Y, John SK. 2020. Bolted and bonded FRP beam-column joints with semi-rigid end conditions. Compos Struct. 247:112500.

Razaqpur AG, Ascione F, Lamberti M, Spadea S, Malagic M. 2019. GFRP hollow column to built-up beam adhesive connection: Mechanical behaviour under quasi-static, cyclic and fatigue loading. Compos Struct. 224(April):111069.

SAC. 1997. Protocol for Fabrication, Inspection, Testing and Documentation of Beam- column Connections and Other Experimental Specimens. Report No. SAC/BD-97/ 02, SAC Joint Venture Sacramento, CA.

Turvey GJ, Cooper C. 1996. Characterisation of the short-term static moment– rotation of bolted connections between pultruded GRP beam and column WF connections. In: El-Badry M, editor. Adv Compos Mater Bridg Struct. [place unknown]: Canadian Society for Civil Engineering; p. 927–934.

Zafari B, Qureshi J, Mottram JT, Rusev R. 2016. Static and fatigue performance of resin injected bolts for a slip and fatigue resistant connection in FRP bridge engineering. Structures. 7:71–84.

Zhang Z, Bai Y, He X, Jin L, Zhu L. 2018. Cyclic performance of bonded sleeve beam-column connections for FRP tubular sections. Compos Part B Eng. 142:171–182.